Experimental and numerical evaluation of metallic compounds for suppressing cup-burner flames

G.T. Linteris [a,*], V.R. Katta [b], F. Takahashi [c]

[a] *Fire Science Division, National Institute of Standards and Technology, 100 Bureau Dr. Stop 8665, Gaithersburg, MD 20899, USA*

[b] *Innovative Scientific Solutions, Inc., 2766 Indian Ripple Road, Dayton, OH 45440-3638, USA*

[c] *National Center for Microgravity Research, NASA Glenn Research Center, Mail Stop 77-5, 21000 Brookpark Road, Cleveland, OH 44135, USA*

Abstract

The first tests of supereffective flame inhibitors blended with CO_2 have been performed in methane–air laminar co-flow diffusion flames stabilized on a cup burner. The CO_2 volume fraction required to extinguish the flames was determined for a range of added catalytic inhibitor volume fractions. When added at low volume fraction, the agents TMT, $Fe(CO)_5$, and MMT were effective at reducing the volume of CO_2 required to extinguish the flames, with performance relative to CF_3Br of 2, 4, and 8, respectively. This performance advantage of the metallic compounds is less than that determined in premixed or counterflow diffusion flames. Further, as the volume fraction of each metallic catalytic inhibitor was increased, the effectiveness diminished rapidly. The greatly reduced marginal effectiveness is believed to be caused by loss of active gas-phase species to condensed-phase particles. Laser-scattering measurements in flames with $Fe(CO)_5/CO_2$ blends detected particles both inside and outside (but not coincident with) the visible flame location for measurement points above the stabilization region. For $Fe(CO)_5$ addition to the air stream at 450 μL/L, the peak scattering cross section for vertically polarized light was 1660 times the value for room-temperature air. The first detailed numerical modeling studies were also performed for methane–air cup-burner flames with CO_2 and $Fe(CO)_5$ added to the oxidizer stream and are used to interpret the experimental results. The role of particles was also illustrated by the numerical results, which showed that significant levels of supersaturation exist in the flame for several of the important iron-containing intermediates. This particle formation is favored in the lower temperature stabilization region of the cup-burner flames, as compared to the higher relevant temperatures of previously described counterflow diffusion flames. The results of this study indicate that the appropriate flame configuration for evaluating the effectiveness of *some* fire suppression agents must be carefully considered, since in those cases, different flame configurations can switch the relative performance of an agent by an order of magnitude.

* Corresponding author. Fax: (301)-975-4052.
 E-mail address: linteris@nist.gov (G.T. Linteris).
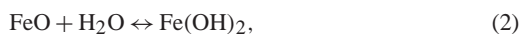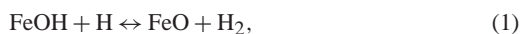
1. Introduction

Finding replacements for the effective but ozone-destroying fire suppressant CF_3Br and related compounds is a continuing research challenge. Metal compounds have attracted attention because some metals recombine radicals in the postcombustion region of premixed H_2/O_2 flames [1] and several metallic compounds are one to two orders of magnitude more effective than CF_3Br at reducing the burning velocity of premixed flames [2–6]. If a means could be found to incorporate such supereffective moieties into a practical fire suppressant (particularly for unoccupied spaces), very effective agents might be possible.

Premixed and counterflow diffusion flames have been used extensively for testing these agents since they provide easily measurable parameters which can be related directly to the effect of the agent on the overall reaction rate. For these supereffective agents, however, few detailed experimental or modeling studies have been conducted with flames resembling fires. The present work remedies this deficiency by presenting results for addition of these highly effective agents to axisymmetric laminar co-flow diffusion flames formed on a cup burner. (The cup burner is typically used with fuels that are liquid; however, it can also be used with those that are gaseous.) Not only do cup burners have flame structures that are a reasonable approximation to those in fires, but they are also widely used by the fire protection industry as a metric to assess fire-suppressant performance [7]. Hence, measurement and numerical prediction of performance of agents in cup burners have clear relevance to their eventual use. The present work examines the performance of metallic agents in cup-burner flames in a fundamental manner by making the first detailed numerical calculations of the flame structure using a 2-D, time-dependent code with full chemistry. These calculations are the first to demonstrate the blowoff phenomenon for the suppression of cup-burner flames caused by a supereffective chemically acting agent.
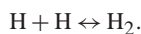
In the experimental results described below, the catalytic agents containing Fe, Mn, and Sn are found to be more effective than CF_3Br when used at low volume fraction. Nonetheless, their performance in the cup burner relative to that in premixed and counterflow diffusion flames is lower than expected based on comparable performance with other catalytic agents. The goal of the present experimental and numerical work is to delineate the performance of these agents in cup-burner flames, examine the blowoff process in cup-burner flames, and provide insight into their predicted effectiveness in suppressing large-scale fires.

2. Background

The flame-inhibition properties of the agents tetramethyltin (TMT, $Sn(CH_3)_4$), methylcyclopentadienyl manganese tricarbonyl (MMT, $CH_3C_5H_4Mn(CO)_3$), ferrocene ($Fe(C_5H_5)_2$), and iron pentacarbonyl ($Fe(CO)_5$) have recently been studied in some detail [5,6,8]. Experiments and modeling of $Fe(CO)_5$ have quantified its performance and explained its mechanism of inhibition for a variety of conditions [8–10]. For iron, strong inhibition is thought to occur from catalytic radical recombination cycles involving iron oxides and hydroxides; for example,

$$FeOH + H \leftrightarrow FeO + H_2, \tag{1}$$

$$FeO + H_2O \leftrightarrow Fe(OH)_2, \tag{2}$$

$$Fe(OH)_2 + H \leftrightarrow FeOH + H_2O, \tag{3}$$

which yield the net reaction

$$H + H \leftrightarrow H_2.$$

For manganese-containing inhibitors, the mechanism is similar (with Mn replacing Fe in the reaction sequence). At low volume fractions, $Fe(CO)_5$ is about 80 times more effective than CF_3Br at reducing the burning velocity of premixed flames; however, at volume fractions above about 100 μL/L,[1] the marginal effectiveness of $Fe(CO)_5$ is greatly reduced. This is believed to occur from condensation of the active iron-containing intermediates to particles [11]. In a similar fashion, MMT loses its effectiveness at about 300 μL/L, and TMT, which is about three times as effective as CF_3Br in premixed flames, loses its marginal effectiveness at about 3000 μL/L. For cup-burner flames, if $Fe(CO)_5$ were added alone to the air stream, it would not be expected to be a particularly effective suppressant because at the high volume fraction of it required for suppression, condensation of active iron-containing intermediates to particles would limit its gas-phase volume fraction, restricting the potential of the gas-phase catalytic cycle. Any practical fire suppressant using these supereffective agents would require some method of overcoming the loss of effectiveness.

One approach to overcoming the loss of effectiveness is to combine catalytic agents with inert compounds. In this case, the overall reaction rate is lowered in part through radical recombination by the catalytic agent, and in part through the lower temperature caused by the added diluent. This approach has been discussed in work since the 1950s [10,12–16], which suggested that combinations of thermally acting and catalytic agents might prove beneficial. These

---

[1] Note that μL/L is equivalent to ppm by volume.

predictions have been confirmed in various studies with premixed and counterflow diffusion flames inhibited by $Fe(CO)_5$ [4], ferrocene [5], CF_3Br [17], phosphorus compounds [18], and alkali metals [19]. Tests and calculations show that addition of an inert compound lowers the temperature and in some cases enhances the performance of the catalytic agent [5]. The goal is to harness the very high efficiency of the metal species at low volume fraction while keeping its concentration below that which causes condensation. Nonetheless, it is generally not known a priori if the combination of an inert agent with the one of the metal-containing catalytic agents will be effective in a particular flame configuration, since the lower temperature can cause higher radical superequilibrium [8], increasing the catalytic effect, but may also provide longer residence times for particle formation [11].

The approach adopted for assessing the effectiveness of the catalytic agents in extinguishing cup-burner flames is to determine how the CO_2 volume fraction required for blowoff changes in the presence of the catalytic inhibitor. This approach is conceptually the same as the classic oxygen index test used to assess material flammability [20]. In that test, the oxygen volume fraction in the air stream at blowoff (i.e., the oxygen index) is determined for solid, liquid, or gaseous fuels with chemical additives in either the fuel or oxidizer. In the present tests, CO_2 (rather than N_2) is added as the diluent to facilitate comparisons with existing experimental data for other configurations. Although previous studies have been performed with heptane and methanol as the fuels [21], the present experiments use methane. A gaseous fuel allows an approximately constant flame size and heat release rate, preserving many properties of the flow field (unlike a liquid-pool fuel, for which fuel supply rate varies with inhibitor addition). These methane–air flames with CO_2 are also essentially nonsooting, which is desirable, since the metal additives would change the production rates of soot (and thus the radiant heat transfer), which would complicate interpretation of the results. The iron, tin, and manganese compounds were selected because there exist recent experimental data on their performance in premixed methane–air flames for comparison. In order to assess the effect of particle formation on the effectiveness of $Fe(CO)_5$ in cup-burner flames, we report the results of laser scattering from particles in a two-dimensional region above the fuel cup. Finally, a time-dependent, 2-D numerical code including full chemistry [22] is used to understand the chemistry and flow-field effects important in stabilization and blowoff of the cup-burner flames inhibited by $Fe(CO)_5$, to investigate the supersaturation conditions of the active iron-containing intermediates,

and to interpret the role of thermophoresis in particle trajectories.

3. Experiment

The cup burner, described previously [23,24], consists of a cylindrical glass cup (28-mm diameter) positioned inside a glass chimney (53.3-cm tall, 9.5-cm diameter). To provide uniform flow, 6-mm glass beads fill the base of the chimney, and 3-mm glass beads (with two 15.8 mesh/cm screens resting on top) fill the fuel cup; the burner cup rim is located 7 cm above the glass beads in the oxidizer stream. Gas flows were measured by mass-flow controllers (Sierra 860[2]), which were calibrated so that their uncertainty was 2% of indicated flow. The methane flow was held constant at 0.342 L/min (fuel-jet mean velocity 0.92 m/s) for all experiments, and the laboratory temperature was $21 \pm 1\,°C$. To determine the blowoff condition, the desired amount of catalytic agent was added to the co-flowing air (held constant at 41.6 L/min, 10.7 cm/s), and CO_2 was added to the flow (in increments of $< 1\%$ near blowoff) until blowoff was observed. The test was repeated at least three times.

The organometallic inhibitors were added to the air stream using multistage saturators in controlled-temperature baths. The $Fe(CO)_5$ and TMT used two-stage saturators of a design described previously [10], while the MMT used a three-stage saturator, with 50% larger stages, to ensure saturation. A measured portion of the added CO_2 flowed as a carrier through each saturator. The volume fraction of the organometallic inhibitors in the air stream was calculated based on the measured air flow, measured carrier gas flow, and calculated vapor pressure of the agent at the bath temperature. The experimental vapor pressure data were obtained from Refs. [25,26]. Since the vapor pressure of MMT is much lower than that of the other agents, the burner and lines were maintained at $> 35.0 \pm 0.5\,°C$ before and during the tests to reduce the likelihood of MMT condensation. Tests to validate the assumption of agent saturation in the carrier gas have been described previously [10]. For bromine as the inhibitor, all flow tubes downstream of agent addition, as well as the burner base, were made of Teflon to avoid reaction. A computer-controlled syringe pump added the liquid Br_2 to a 2.1-m-long tube

carrying the air and CO_2, and complete Br_2 evaporation was observed to occur within a tubing length of less than 1 m.

The fuel gas is methane (Matheson UHP, 99.9%), and the air is house compressed air (filtered and dried), which is additionally cleaned by passing it through a 0.01-μm filter, a carbon filter, and a desiccant bed to remove small aerosols, organic vapors, and water vapor. The chemicals used were $Fe(CO)_5$ (Aldrich), TMT (Alfa Aesar), MMT (Alfa Aesar), CH_3OH (Aldrich, 99.8%), Br_2 (Aldrich, 99.5%), CF_3Br (Great Lakes), N_2 (boil-off), and CO_2 (Airgas).

For the particle measurements, a 90° laser-scattering system was used, as described in previous work [10,27]. A 5-W argon ion laser operating at 488 nm supplied the laser light to a single-mode fiber, which carried the beam to an optical table in a fume hood. To prevent laser light from scattering off of the cup-burner chimney walls, the round cup-burner chimney (9.5-cm diameter) was cut off to a height of 10 cm, which was 2 mm below the fuel cup rim; the cup burner and shortened chimney were then inserted into a larger square chimney (13 × 13 cm). This square chimney was identical to that used in the previous scattering measurements made with a premixed nozzle burner described in Ref. [11], except that brass straightening screens were installed in the concentric region between the square chimney and the round chimney, and a second co-flow of air was added at the same velocity as in the inner, round co-flowing air stream of the cup burner. The square chimney allowed use of rubber bellows, which connect the experimental burner to the optical components, thereby introducing the laser light and collecting the scattered light while avoiding reflections from windows (see Ref. [11] for details). A three-axis translator positioned the burner and chimney in the stationary optical path. The scattering measurements were made on horizontal paths across the flame at fixed heights above the fuel-cup rim. Tests with gases of known scattering cross section [28] provided the calibration factors for the optical system.

An uncertainty analysis was performed, consisting of calculation of individual uncertainty components and root-mean-square summation of components. All uncertainties are reported as *expanded uncertainties* $X \pm ku_c$, from a combined standard uncertainty (estimated standard deviation) u_c and a coverage factor $k = 2$ (confidence level 95%). Likewise, when reported, the relative uncertainty is ku_c/X. The expanded relative uncertainties for the experimentally determined quantities in this study are CO_2 volume fraction, 4%; and inhibitor volume fraction for organometallics, CF_3Br, and Br_2, 5, 2.7, and 2.0%, respectively.

4. Numerical model

A time-dependent, axisymmetric mathematical model known as UNICORN (unsteady ignition and combustion using reactions) was used for simulation of the cup-burner flames. This model solves the two-dimensional equations of momentum, continuity, enthalpy conservation, and species conservation. The body-force term due to gravity is included in the axial-momentum equation. A clustered mesh system is employed to trace the gradients in flow variables near the flame surface. The kinetic mechanism consisted of a hydrocarbon mechanism from GRI-V1.2 together with an iron-species submechanism [8]. The rate of the reaction $CH_3 + H + M \rightarrow CH_4 + M$ was changed from the GRI value to that of Warnatz [29], since it yielded better agreement with existing experimental data for both counterflow diffusion flame extinction [30] and co-flow jet diffusion flame blowoff [31]. The thermophysical properties such as enthalpy, viscosity, thermal conductivity, and binary molecular diffusion of all of the species are calculated from polynomial curve fits. Mixture viscosity and thermal conductivity are then estimated using the Wilke and Kee expressions [32], respectively. Diffusion velocities are calculated based on Fick's law. For each species, an effective diffusion coefficient in the local mixture is calculated using mixture rules and the binary diffusion coefficient for each diffusion pair [33]. A broadband radiation model [34] based on the assumption of optically thin media was incorporated into the energy equation. Only radiation from CH_4, CO, CO_2, and H_2O was considered in the present study. (Note: we did not include radiation from and chemical reaction of particles, however, trajectory calculations for them are described below.) Details of the numerical solution technique as well as the boundary conditions are the same as described in earlier publications [35].

The capabilities of the numerical model were validated through comparisons with experimental data for both counterflow and co-flow diffusion flames. For the methane–air counterflow flames, the global extinction strain rate calculated using the present two-dimensional, time-dependent code with the adopted kinetic mechanism was 640 s^{-1}, compared to the experimental value of 610 ± 40 s^{-1} [9]. (Note: A known problem with comparing experimental results of counterflow jet diffusion flames with the results of 1-D calculations is that the actual boundary conditions in the experiment are intermediate between the modeled plug flow and potential flow inlet conditions [36]. With the present 2-D code, however, the upstream boundary conditions on the fuel and oxidizer flows are accurately modeled, and the usual interpolations done with the 1-D calculated results

Table 1

Blowoff volume fraction for CO_2 $X_{CO_2,bo}$ in a methane–air cup burner with and without added $Fe(CO)_5$ or CF_3Br in the air or fuel stream

Catalytic inhibitor	X_{inh}	Inhibitor location	$X_{CO_2,bo}$ (%)	% reduction in $X_{CO_2,bo}$
None	—	—	15.7 ± 0.6	0
$Fe(CO)_5$	450 µL/L	In air	14.1 ± 0.6	9.6 ± 0.5
$Fe(CO)_5$	924 µL/L	In air	13.5 ± 0.5	13.5 ± 0.8
$Fe(CO)_5$	450 µL/L	In air w/1% CH_4	14.0 ± 0.6	10.7 ± 0.6
$Fe(CO)_5$	450 µL/L	In fuel	15.4 ± 0.6	1.3 ± 0.1
$Fe(CO)_5$	4500 µL/L	In fuel	15.2 ± 0.6	2.6 ± 0.2
CF_3Br	1.3%	In air	4.4 ± 0.2	72.0 ± 4.1
CF_3Br	11.0%	In fuel	8.7 ± 0.3	44.2 ± 2.5

are not necessary.) Code validation has also been performed in co-flow diffusion flames. In previous work, the calculated co-flow air velocity required to produce flame lift-off was approximately 0.8 m/s (for a methane jet velocity of 1.7 m/s) [31], while the experimental value was 0.76 m/s [37]. In recent work with cup-burner flames, the volume fraction of CO_2 required for flame blowoff was calculated to be 14.5 or 16.5% (with the above-mentioned changes in the CH_3 reaction kinetics parameters) and measured to be $15.7 \pm 0.6\%$ [35], while for the chemically acting agent CF_3H, these values were 10.1 and $11.7 \pm 0.8\%$ [38]. The code was also able to reproduce both the flame-tip flicker frequency and the flame-base oscillation. These results illustrate the present model's ability to predict flame extinguishments for a variety of configurations and agents.

5. Experimental results

In the first tests, the amount of CO_2 required for suppression of the cup-burner flame was determined with $Fe(CO)_5$ added to either the air or methane stream. Table 1 summarizes the results. The top line shows that for CO_2 alone, the volume fraction of CO_2 in the air stream for blowoff $X_{CO_2,bo}$ is 15.7 ± 0.6. The next two lines show that addition of $Fe(CO)_5$ to the air stream at relatively high volume fractions (450 or 924 µL/L) causes only a 9.6 ± 0.5 or $13.5 \pm 0.8\%$ reduction in $X_{CO_2,bo}$. If we add 1% CH_4 to the air stream to change the flame location and hence the scalar dissipation rate, the reduction in $X_{CO_2,bo}$ with addition of 450 µL/L of $Fe(CO)_5$ is slightly greater, but still only about $10.7 \pm 0.6\%$. Likewise, addition of $Fe(CO)_5$ to the fuel stream at either 450 or 4500 µL/L causes only a 1.3 ± 0.1 or $2.6 \pm 0.2\%$ reduction in the amount of CO_2 required for blowoff. These results are quite different from those in either premixed or counterflow diffusion flames, for which $Fe(CO)_5$ is a very strong inhibitor [2–5,8]. These results are surprising, since a correlation between the flame-inhibiting behavior of additives in premixed flames and that in diffusion flames has been discussed repeatedly in the literature [39–48].

The agent CF_3Br is also a strong catalytic radical scavenging agent. As a test of the validity of the present approach, $X_{CO_2,bo}$ was determined with CF_3Br added to either the fuel or the air stream at a volume fraction, which would halve the burning velocity of a premixed flame. These results are shown at the bottom of Table 1. In contrast to the results with $Fe(CO)_5$, addition of CF_3Br to either stream has a large effect on $X_{CO_2,bo}$, a reduction by a factor of 2 to 3. Clearly, CF_3Br and $Fe(CO)_5$ behave differently in the cup burner with respect to their ability to reduce the CO_2 requirement for blowoff.

The results in Table 1 may lead one to conclude that although $Fe(CO)_5$ is highly effective in premixed flames, it has little effect in cup-burner flames. Conducting cup-burner blowoff tests with added CO_2 for a *continuous* range of concentrations of $Fe(CO)_5$ in the air stream, however, shows that $Fe(CO)_5$ does, in fact, inhibit the flame quite strongly (although much less than expected based on premixed and counterflow diffusion flame results). Fig. 1 shows the volume fraction of CO_2 required for blowoff as a function of the initial volume fraction of the catalytic inhibitor in the air stream (prior to CO_2 addition). Data are presented for $Fe(CO)_5$, as well as for the organometallic agents TMT and MMT. For comparison, tests were also performed for Br_2 and CF_3Br. For blowoff of these methane–air flames, pure CO_2 is required in the air stream at a volume fraction of $15.7 \pm 0.6\%$, whereas CF_3Br, a catalytic agent, is required at $2.4 \pm 0.1\%$. Moreover, as Fig. 1 shows, adding CF_3Br at volume fractions below the blowoff value greatly reduces the amount of CO_2 required for blowoff. For example, adding half of the blowoff value of CF_3Br reduces the amount of CO_2 required by 70%. The curvature in the line for CF_3Br in Fig. 1 indicates that, as described previously [15], the combination of CF_3Br and CO_2
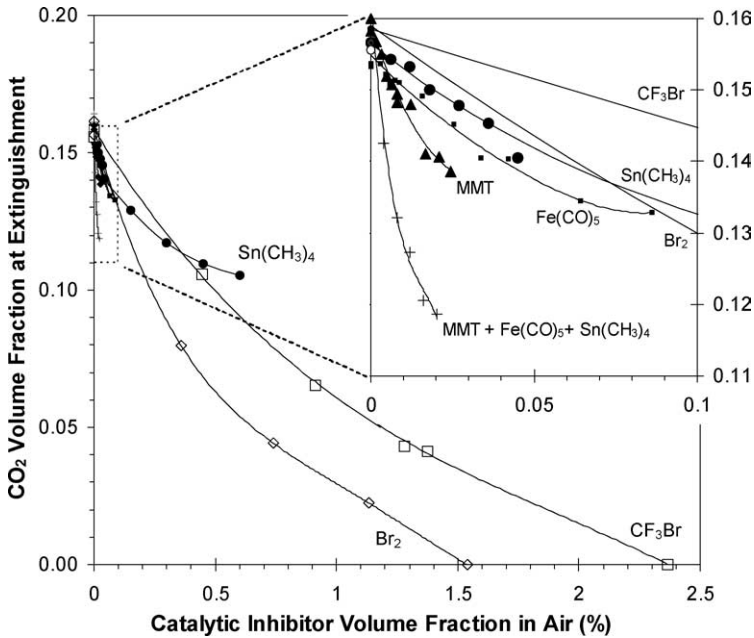
Fig. 1. Volume fraction of CO_2 required for methane–air cup-burner flame blowoff vs catalytic inhibitor volume fraction, CF_3Br, Br_2, $Fe(CO)_5$, TMT, MMT, or a blend of the last three. The boxed region in the upper left is expanded in the inset, and in it, the data for the MMT, $Fe(CO)_5$, and TMT blend are plotted as a function of the MMT volume fraction.

is synergistic; that is, when combined, less of each is required for blowoff than one would expect based on a linear interpolation of the individual results.

The inset to Fig. 1 shows the data for the organometallic agents in more detail and indicates that at low volume fraction, the organometallic agents are actually *more* effective than CF_3Br. For the sequence CF_3Br, TMT, $Fe(CO)_5$, and MMT, the relative magnitudes of the slopes of the curves (at low volume fraction) are 1, 2, 4, and 8, so that $Fe(CO)_5$ is about four times as effective as CF_3Br. While this performance is noteworthy, it is far less than was observed in premixed flames or counterflow diffusion flames, for which the benefit was one to two orders of magnitude for $Fe(CO)_5$ as compared to CF_3Br. Also, the relative performance of $Fe(CO)_5$ and MMT is switched, with $Fe(CO)_5$ about twice as effective as MMT in premixed flames, while the opposite is true for the present cup-burner flames. Especially apparent in the inset to Fig. 1 is that the curves for each of the three agents, TMT, $Fe(CO)_5$, and MMT, all have a decreasing slope as their volume fraction increases. This behavior is similar to that in premixed and diffusion flames in which the loss of effectiveness was shown to be due to condensation of active species.

In previous work it has been argued that to obtain good performance by the supereffective agents, it might be possible to add small, noncondensing amounts of several catalytic agents together with an inert agent [10]. We tested this claim by adding a blend of the three catalytic metals MMT, $Fe(CO)_5$, and TMT to the air stream and then finding $X_{CO_2,bo}$. The bottom curve in the inset to Fig. 1 shows $X_{CO_2,bo}$ for such a blend. MMT, $Fe(CO)_5$, and TMT are present in the molar ratio 1:2.1:15.5, and the curve is plotted as a function of the MMT volume fraction. Note that at the test point of the highest volume fraction, the three agents are added at 200, 420, and 3100 μL/L, respectively. (These values were selected since the individual curve for each agent is roughly linear up to these volume fractions; i.e., they have not yet drastically lost their marginal effectiveness.) As shown, the agents do work together to reduce the amount of CO_2 required for blowoff, and, up to the maximum volume fractions added, the blend does not drastically lose its effectiveness. Amazingly, however, with addition of *three* catalytic inhibitors, *each* at a volume fraction which would easily reduce the overall reaction rate in a premixed flame by a factor of 4, and each used below the volume fraction at which the agent alone starts to have greatly reduced effectiveness, the combination still reduces the amount of CO_2 required for blowoff by only 25%.

Addition of the metallic agents containing Sn, Mn, and Fe to the cup-burner flame leads to the formation of particles in the flow. Bandpass filters were used to verify that the visual emission, which occurs both inside and outside the blue flame region (from peak CH emission), was graybody rather than due to atomic transitions. Nonetheless, to more accurately
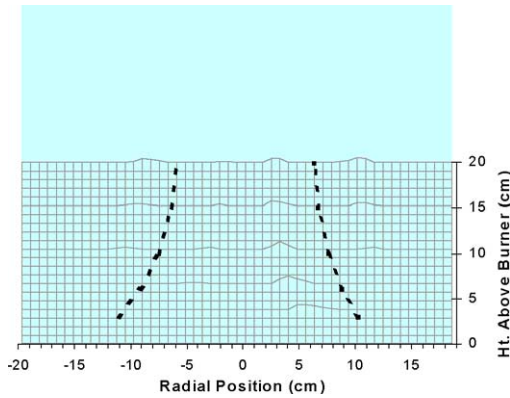
Fig. 2. Scattering cross section for laser light at 488 nm as a function of radial position and height above burner in methane–air cup-burner flame with 8% CO_2 and $Fe(CO)_5$ in air at specified volume fraction. Dotted lines show flame location from a digitized video image of the uninhibited flame. $Fe(CO)_5$ in air at 100 μL/L.
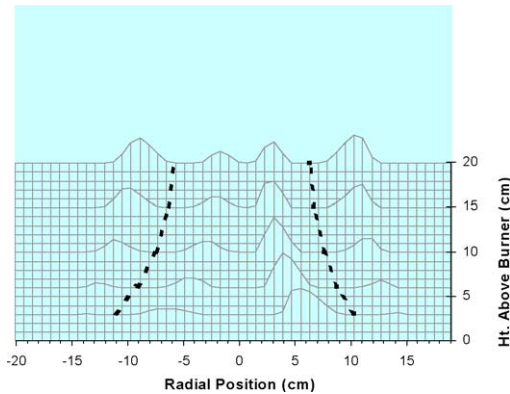

Fig. 4. Scattering cross section for laser light at 488 nm as a function of radial position and height above burner in methane–air cup-burner flame with 8% CO_2 and $Fe(CO)_5$ in air at specified volume fraction. Dotted lines show flame location from a digitized video image of the uninhibited flame. $Fe(CO)_5$ in air at 325 μL/L.

Fig. 3. Scattering cross section for laser light at 488 nm as a function of radial position and height above burner in methane–air cup-burner flame with 8% CO_2 and $Fe(CO)_5$ in air at specified volume fraction. Dotted lines show flame location from a digitized video image of the uninhibited flame. $Fe(CO)_5$ in air at 200 μL/L.
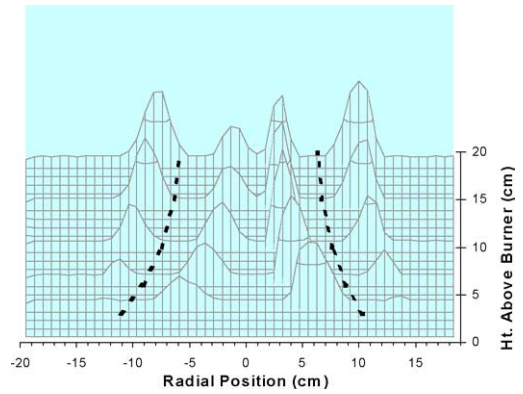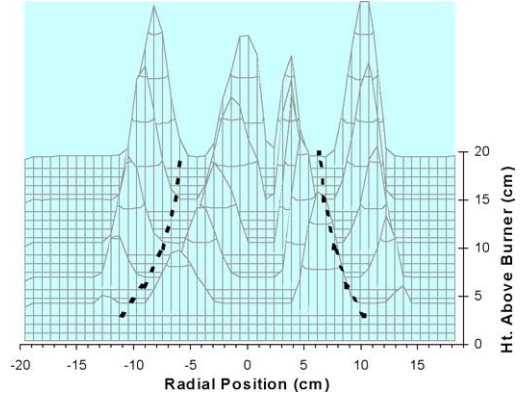

Fig. 5. Scattering cross section for laser light at 488 nm as a function of radial position and height above burner in methane–air cup-burner flame with 8% CO_2 and $Fe(CO)_5$ in air at specified volume fraction. Dotted lines show flame location from a digitized video image of the uninhibited flame. $Fe(CO)_5$ in air at 450 μL/L.

detect the particles, we conducted laser-scattering experiments in the cup-burner flames with and without added $Fe(CO)_5$. The scattering measurements were made on several horizontal paths across the flame at fixed heights above the fuel-cup rim. Although pure methane–air cup-burner flames are unsteady, flickering at about 10 Hz with a large amplitude, flames with sufficient added CO_2 are steady, nearly nonflickering, and nonsooting. Hence, scattering measurements in cup-burner flames with $Fe(CO)_5$ added to the air stream were performed with a CO_2 volume fraction of 8% in the total oxidizer stream flow. This approach was reasonable since the blowoff tests were also conducted with appreciable volume fractions of CO_2.

The agent $Fe(CO)_5$ was added at 0, 100, 200, 325, and 450 μL/L to the air stream, which was then combined with the CO_2. Figs. 2 to 5 present radial profiles of the scattering cross section (arbitrary but consistent units) at heights above the burner rim of 3, 6, 10, 15, and 20 mm. Also shown in each figure is the location of the peak visible emission, obtained from a digitized video image of the flame with 0 μL/L of $Fe(CO)_5$. Since the oxygen demand of the $Fe(CO)_5$ in the oxidizer stream at 450 μL/L is about 0.6% that of the methane, the flame location should not be significantly modified by the presence of this fuel-like agent in the co-flow [49]. In Figs. 2 to 5, the peak scattering signal detected is 1.1, 4.7, 12.7, and

25.5×10^{-6} (cm-sr)$^{-1}$, respectively, which is 50, 209, 559, and 1660 times the scattering signal for air under laboratory conditions. In all cases, the presence of particles is clearly indicated, and the magnitude of the scattering signal increases with the $Fe(CO)_5$ volume fraction in air. For each value of X_{inh}, the relative distribution of the particles for each height and radial position is approximately conserved. Particles are present both inside and outside, but not coincident with, the visible flame location. Flames without $Fe(CO)_5$ (not shown) had scattering cross sections attributable to only the hot and cold product and reactant gases; i.e., no scattering from soot was detected. The slight radial asymmetry in the scattering data of Figs. 2 to 5 may occur from burner asymmetry, i.e., from imperfections in the glass burner cup or the glass beads it contains or slight off-center location of the flow-straightening screens (which sometimes shift radially by up to 1 mm during the experiment).

6. Numerical results

The numerical model is able to predict many features of the flame, including the temperature and species concentration profiles and the fluid velocity vectors as a function of time and position. For example, Fig. 6 shows the blowoff condition predicted by the model. Two-dimensional color maps of the temperature are presented for 10% CO_2 and 0.011% $Fe(CO)_5$ in oxidizer (left) and 10% CO_2 and 0.012% $Fe(CO)_5$ in oxidizer (right). The figures indicate that, unlike counterflow diffusion flames, for which the extinction occurs essentially globally, cup-burner flames blow off due to a localized disruption of the stabilization. For the conditions of the figure, the model predicts that the cup-burner flame will blow off when the $Fe(CO)_5$ volume fraction is 0.014%.

The blowoff condition for various methane/air/CO_2/$Fe(CO)_5$ flames was determined with the numerical model. The time-dependent calculation is run for separate cases involving increasing volume fractions of the inhibitor in the air stream. At some specific value of the inhibitor volume fraction, the flame detaches from the burner, drifts downstream, and exits the computational domain. This is the blowoff volume fraction. The model predicts a blowoff volume fraction of 1400 μL/L for the case of $Fe(CO)_5$ alone (i.e., no CO_2) in the air stream of the cup burner. As described above, experiments with $Fe(CO)_5$ added to pure methane–air cup-burner flames were not conducted since flames with such high volume fractions of $Fe(CO)_5$ would clearly be expected to lead to strong condensation of the iron-containing intermediates. Instead, experiments and calculations were performed to determine the effect of increasing levels
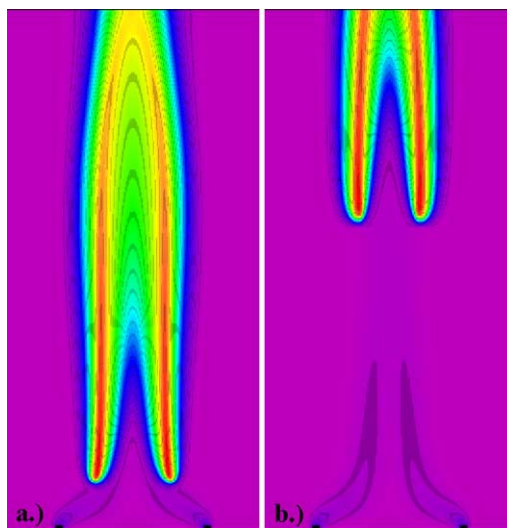

Fig. 6. Two-dimensional map of calculated temperature in cup-burner methane–air flames with 10% CO_2 in the oxidizer stream, and (a) 0.011 and (b) 0.012% $Fe(CO)_5$ volume fraction in the air stream, illustrating the blowoff phenomenon.

of $Fe(CO)_5$ in the air stream on the volume fraction of CO_2 required to produce blowoff. Fig. 7 shows the experimental data (from Fig. 1) for $Fe(CO)_5$ together with those predicted from the numerical calculations. As the figure shows, the numerical results show much stronger initial inhibition of the flame (at low $Fe(CO)_5$ volume fraction), as well as a much smaller loss of effectiveness (flattening out of the curve) for increasing $Fe(CO)_5$ volume fractions. Possible reasons for these discrepancies are discussed in detail below.

7. Discussion

7.1. Comparative inhibitor effectiveness in different flames

The variation in the performance advantage of the chemically acting inhibitors relative to other agents, and how it varies with the flame metric used to assess performance, can be investigated further (see Table 2). The agents, listed across the top, are CO_2, CF_3H, CF_3Br, Br_2, TMT, MMT, and $Fe(CO)_5$, which represent an increasing degree of interference in the flame chemistry as the dominant mode of flame inhibition. As for the flame metric to assess agent effectiveness, we consider premixed, counterflow diffusion and co-flow diffusion (cup-burner) flames. With the premixed flames, an often-used metric is the amount of inhibitor needed to reduce the flame speed of stoichiometric flames by 30% (which corresponds to a
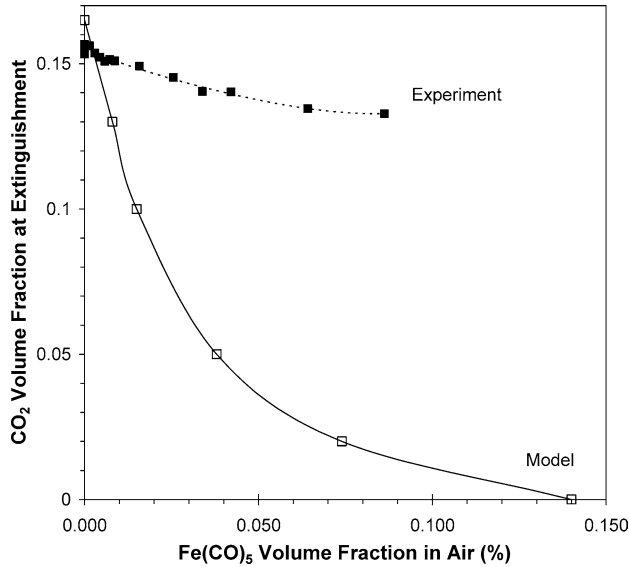
Fig. 7. Measured and predicted CO_2 volume fraction in the oxidizer stream required for blowoff of a methane–air cup-burner flame as a function of the $Fe(CO)_5$ volume fraction in the air.

Table 2
Performance advantage of chemical agents as compared to CO_2 using various flame metrics

Inhibition metric	X_{CO_2} (%)	Performance of this agent, relative to CO_2 (X_{CO_2}/X_i)						
		CF_3H	CF_3Br	Br_2	TMT	MMT	$Fe(CO)_5$	$Fe(CO)_5$ (calc)
Premixed flames								
X_i for 10% red in S_L	1.36	2.4	6.8	5.0[a]	26	360	660	
X_i for 30% red in S_L	4.61	2.0	8.5	9.7[a]	25	351	698	
X_i for 45% red in S_L	7.78	2.0	9.6		22	294	622	
Counterflow diffusion flames								
X_i for extinction at $a = 550$ s^{-1}	1.30	3	7				245	406
X_i for extinction at $a = 490$ s^{-1}	2.11	1.7	5.0				127	301
X_i for extinction at $a = 430$ s^{-1}	2.75	1.3	4.0				62	250
X_i for extinction at $a = 300$ s^{-1}	3.83	0.9	5.6					
X_i for extinction at $a = 80$ s^{-1}	13.8		5.4					
X_i for extinction at $a = 50$ s^{-1}	17.0		4.6					
Cup-burner flames								
X_i for blowoff	15.7	1.4	6.4	10.2				116
X_i to achieve a 10% reduction in CO_2 required for blowoff	1.8	2.5	14.6	36	34	113	49	454

Source. Data from Refs. [2,4–6,51–55].
[a] Br_2 premixed flame data are for n-hexane–air flame at $\phi = 0.95$.

factor of 2 reduction in overall reaction rate) [2]. We adopted this value, but also determined the amount of agent necessary to achieve a 10% and a 45% reduction in flame speed. Similarly, for counterflow diffusion flames, we determine the amount of agent required to achieve extinction at global strain rates [50] of 550, 490, 430, 300, 80, and 50 s^{-1}. For the co-flow diffusion flames, we determine the volume fraction of pure agent necessary to cause flame blowoff and also

the volume fraction of agent required to reduce the CO_2 required for blowoff by 10% (since this allows us to assess the potential of blends of catalytic and inert agents). For each flame metric, Table 2 shows the performance of each agent i relative to CO_2 (X_{CO_2}/X_i for the same amount of inhibition). The values of the agent volume fraction required were determined from curve fits to the experimental data provided in Refs. [2,4–6,51–55]. For reference, the volume frac-

tion of CO_2 used in the normalizations is listed in the second column of the table. For example, at 30% reduction in the flame speed requires a CO_2 volume fraction of 4.61%, and a 10% reduction in the amount of CO_2 required for flame blowoff of the cup burner requires 1.8% (= $(0.1 \cdot 15.7\%)/(1–0.9 \cdot 0.157)$, where the additive volume fraction is based on the air only).

In Table 2, the roles of both residence time in the flame and the chemical activity of the agent are illustrated. For example, across each row, the residence time is approximately constant. That is, for each row, the premixed flame speed is constant, or the counterflow diffusion flame global strain rate is constant, or the fuel and oxidizer flow rates in the cup-burner diffusion flames are constant. Hence, the relevant flow times are nearly constant for each row, and for these metrics, the flow time matches the chemical time under these conditions. Across each row, the table shows the performance advantage of that agent over CO_2 under the condition of the same residence time; going down the rows typically shows the effect of increasing residence time. As described in Ref. [56], correspondence has been illustrated between the low-strain (50 s^{-1}) counterflow extinction values and the cup-burner blowoff values for heptane–air flames with hydrofluorocarbons or CF_3Br added to the air stream. For this reason, low-strain results available for CO_2 and CF_3Br in methane–air flames [55] are also listed in Table 2 at strains of 50 and 80 s^{-1}.

In premixed flames (the first three lines of Table 2), the radical-trapping agent CF_3H is only about twice as effective as the thermally acting agent CO_2, while the catalytic agents CF_3Br, and Br_2 are about 5 to 10 times as effective, and the catalytic metal agents TMT, MMT, and $Fe(CO)_5$ are 25 to 700 times as effective. Their effectiveness at the different residence times of these premixed flames varies by at most a factor of 2. In the counterflow diffusion flames, the agents CF_3H and CF_3Br have reduced marginal effectiveness at higher strain (lower residence time) [53], which drops off faster than that of CO_2 [51] for CF_3H, but at about the same rate for CF_3Br. For $Fe(CO)_5$, in the counterflow flames, the performance advantage over CO_2 drops by a factor of 4 as the strain rate drops by only 20%. This has been described as being due to longer residence times for particle formation which occur in the lower-strain counterflow diffusion flames [27,57].

For causing the blowoff of the cup-burner diffusion flames, the performance advantages of CF_3H, CF_3Br, and Br_2 over CO_2 are about the same (generally about 30% of their advantage over CO_2 in premixed and counterflow diffusion flames). As described above, tests were not performed for pure organometallic agents in the cup burner since for the high volume fractions of agents required, condensation of metal species and poor performance were expected. As additives to reduce the amount of CO_2 required to cause blowoff, however, these three agents are performing better than in the co-flow diffusion flames. Similar results hold for Br_2. These results are consistent with the enhanced performance of catalytic agents in the presence of an inert compound as described in Refs. [10,12–16]. This was not the case, however, for MMT and $Fe(CO)_5$, which both had much poorer performance relative to CO_2 in the diluted cup-burner flames, as compared to their performance in the premixed flames. Since unwanted fires may most closely resemble cup-burner flames, it is of interest to explore why these very effective agents were not very effective in the cup burner—even when added at low volume fraction.

One approach to investigating the deviation (lowering) in the performance index for $Fe(CO)_5$ for the counterflow and co-flow diffusion flames as compared to the premixed flame metrics is to use the numerical model to estimate the performance that would have occurred in the counterflow and co-flow diffusion flames in the absence of condensation of intermediate species. To do this, we apply the gas-phase-only numerical model to predict the blowoff condition for the cup-burner and extinction of the counterflow flame. The results are shown in the last column of Table 2. As the table shows, the variation in the performance advantage over CO_2 is much greater in the gas-phase-only calculation than in the experiments, and is much closer to that for the premixed flames. For cup-burner flames, the performance relative to CO_2 is again higher in the calculated case than in the experiment for the amount of agent to achieve a 10% reduction in the required CO_2 for blowoff. These results illustrate that without the loss of effectiveness (attributable to condensation) the performance advantage of these agents predicted by the numerical calculations is fairly consistent across flame types and degree of inhibition in each (note that the numerical model predicts the premixed flame results well for flame speed reductions below 45% [8]).

7.2. Cup-burner performance of metallic agents

Performance of $Fe(CO)_5$ in the cup burner can be evaluated through examination of the numerically calculated flame structure. Fig. 8 shows the temperature field (color scale) and velocity vectors for cup-burner flames with 10% CO_2 in the oxidizer stream with (left) and without (right) $Fe(CO)_5$ added at a volume fraction of 100 μL/L in the air. The flame with $Fe(CO)_5$ is shifted significantly downstream compared to the flame without, allowing appreciable flow of the agent-laden oxidizer stream into the fuel side
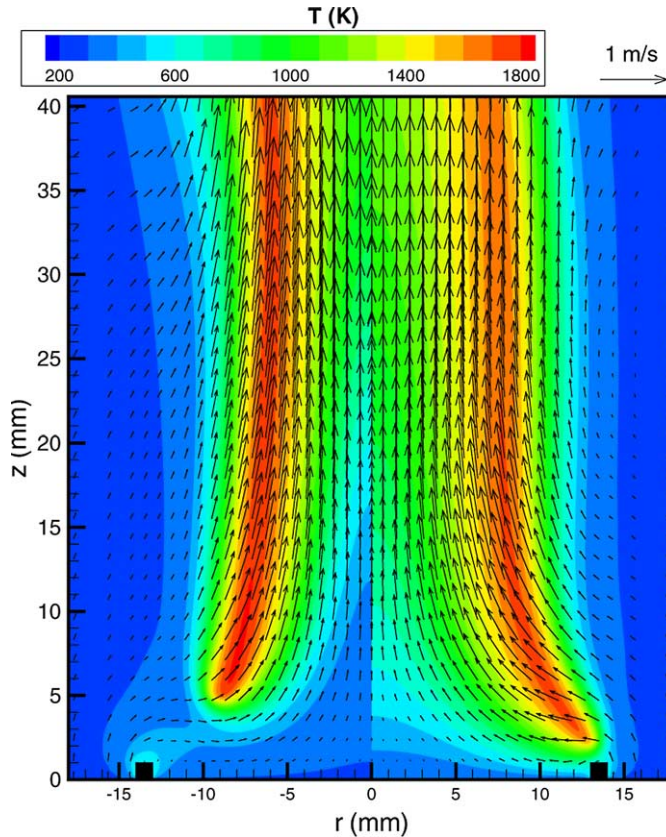
Fig. 8. Calculated temperature (color scale) and velocity vectors (arrows) for methane–air cup-burner flame with an oxidizer stream CO_2 volume fraction of 10%, with (left) and without (right) an added $Fe(CO)_5$ volume fraction of 100 μL/L.

of the flame base. The temperature of this stream is also relatively low, $\lesssim 600$ K. As shown in Fig. 9, this allows significant amounts of $Fe(CO)_5$ to flow into the fuel side prior to decomposition, easily reconciling the large scattering signal both inside and outside the peak temperature region of the flame. As Fig. 9 also shows, the $Fe(CO)_5$ starts to decompose at a relatively low temperature (< 500 K). As illustrated by reactions (1) to (3) above, the significant species for the cycle of flame inhibition by iron compounds are FeO, FeOH, and $Fe(OH)_2$. The volume fraction of FeOH is shown in Fig. 9, while those for OH, Fe, and $Fe(OH)_2$ are depicted in Fig. 10. Note that the volume fraction profile for FeOH mimics that of FeO, but since its thermodynamics has a lower temperature sensitivity [6], the volume fraction contour has a wider profile. As shown, $Fe(OH)_2$ tends to be located outside the region of peak temperature, while OH, Fe, and FeO tend to be within that region. For OH, this occurs since this is where the high-activation-energy chain-branching reactions are occurring. For Fe, FeO, and $Fe(OH)_2$, their distribution is determined primarily by equilibrium thermodynamic considerations [6]: Fe and FeO, and FeOH are favored at high temper-

atures, while $Fe(OH)_2$ is favored at lower temperatures. For $Fe(OH)_2$, volume fraction is also lowered near the locus of peak temperature due to reaction with H atoms.

As shown in Fig. 6, an important feature of cup-burner flames is that the destabilization (blowoff) phenomenon is different from the global extinction of a counterflow diffusion flame. In a previous paper [58], a region of peak reactivity (the reaction kernel) which formed in the flame base region was found to be responsible for the flame stabilization and destabilization, and this reaction kernel is at a much lower temperature (~ 1550 K) [31] than either the downstream region of the flame (~ 1800 K), or other flames such as premixed or counterflow diffusion flames. This unique feature of the cup-burner flame structure and blowoff process has the consequence of potentially greater condensation of intermediate metal-containing species with subsequent loss of effectiveness. Another result is that manganese could be more effective at lower temperatures. Examination of the equilibrium volume fractions of iron- and manganese-containing species in hydrocarbon systems presented in Ref. [6] reveals that the equilibrium volume frac-
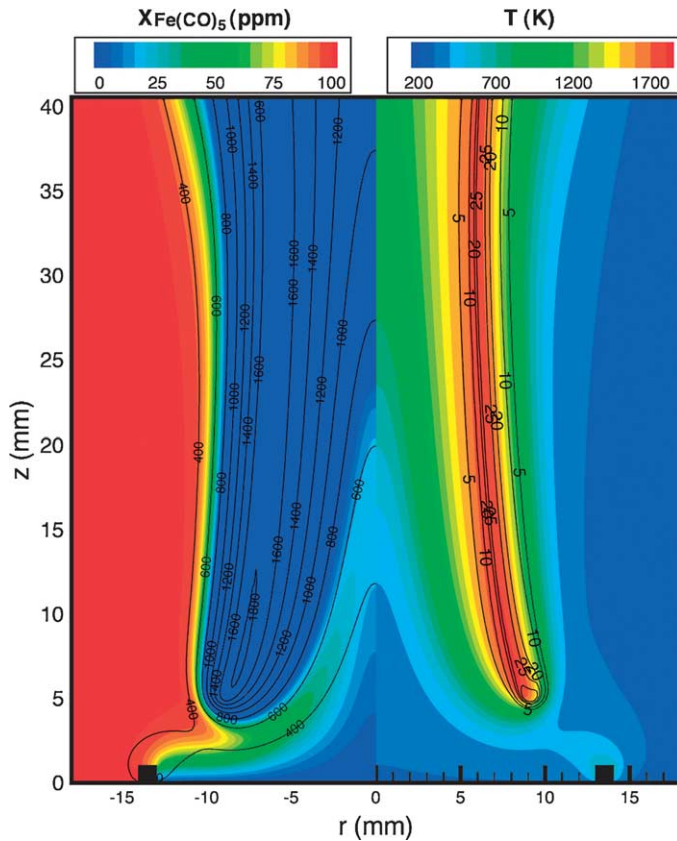
Fig. 9. Methane–air flame with CO_2 and $Fe(CO)_5$ volume fractions of 0.10 and 100 μL/L in the oxidizer stream. (Left) $Fe(CO)_5$ volume fraction (color scale) and temperature contours; (right) temperature (color scale) and contours of FeOH volume fraction in μL/L.

tions of important intermediate species for the manganese system (MnO and MnOH) are favored over the equivalent species in the iron system (FeO and FeOH) when evaluated at 1550 K as compared to 1800 K. Further, the species $Mn(OH)_2$, which is required at a relatively high volume fraction for effective inhibition, becomes increasingly favored at lower temperature, removing the bottleneck for Mn inhibition, which occurs near 2000 K. This can reconcile the superior performance of MMT over $Fe(CO)_5$ in the cup burner (lower temperature) as compared to that in premixed flames.

Although the organometallic compounds *are* effective at reducing the amount of CO_2 required for cup-burner blowoff as compared to CF_3Br, their relative performance is drastically poorer than one would expect based on their behavior in premixed flames, and it is of interest to try to understand why. Two possible causes of the loss of effectiveness are the same as were discussed previously for premixed and counterflow diffusion flames, namely, (1) saturation of the catalytic cycles and (2) condensation of active gas-phase species. The saturation of the cat-

alytic cycles is defined as a state in which the chain-carrying flame radicals have already been reduced to near-equilibrium levels, so that additional catalytic inhibitor has no further benefit. This explanation of the lack of effectiveness is deemed to be unlikely, based on two results shown in Fig. 1: those for Br_2, and those for the blend of MMT, $Fe(CO)_5$, and TMT. The experiments with Br_2 were designed to test the action of a catalytic agent without the confounding effects of condensation of inhibiting species. Further, it is an improvement over tests with CF_3Br for this purpose, since CF_3Br, because of its carbon content and use at relatively high volume fraction ($> 2\%$), can have fuel-like behavior, moving the flame location, changing the scalar dissipation rate, and affecting the blowoff condition. Bromine, added at half the volume fraction, and having no reducing species, does not have a fuel effect. As Fig. 1 shows, the curve for Br_2 is linearly decreasing in the region where the other curves are starting to flatten out—that is, it keeps working, implying that radical depletion is not the cause of the loss of effectiveness of the metals (otherwise, Br_2 would stop working at about the same
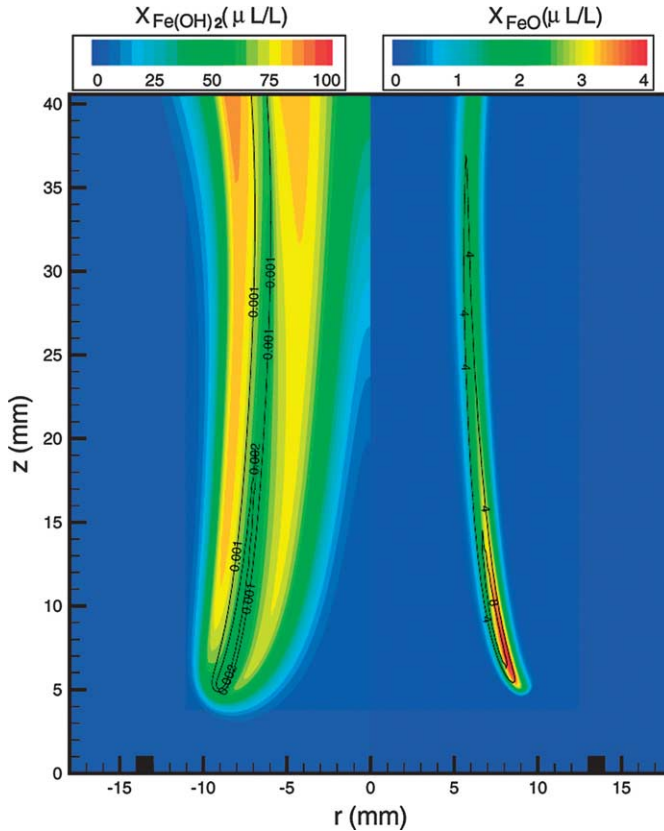
Fig. 10. Calculated volume fractions (μL/L) of (left) Fe(OH)$_2$ (color scale) and OH (contours); (right) FeO (color scale) and Fe (contours).

value of $X_{CO_2,bo}$). Note that although catalytic radical recombination cycles can be more or less effective in certain temperature regimes due to inhibition reaction thermodynamics [13,59], the iron cycle tends to work over a wide range of temperatures; its effectiveness varies primarily with the location of the radicals to recombine [60]. Hence, if it were saturated, the radicals would be at equilibrium levels throughout the flame, and other catalytic agents (such as those containing Br) which only work in certain regimes would still not work. The data for the blend of metallic inhibitors show a similar result. If each of the agents added alone was losing its effectiveness due to radical depletion, adding a second (or third) catalytic agent to the mix would not provide additional inhibition (since radicals would already be reduced to their equilibrium levels). In the bottom curve of the inset to Fig. 1, however, the blend of all three agents clearly shows additional inhibition over MMT alone, providing evidence against saturation of the radical scavenging by the metals. Finally, the numerical results for flames with increasing amounts of Fe(CO)$_5$ in the air stream can be examined to determine the H-atom superequilibrium. For flames with 100 μL/L of Fe(CO)$_5$, the

ratio of [H] to [H]$_{equil}$ is about 2500, clearly indicating that the radicals have not approached their equilibrium levels, so that the loss of effectiveness must be caused by another effect.

Condensation to particles is more likely the cause of the degraded performance of the metal agents. Evidence to support this is that the approximate agent volume fraction for the loss of effectiveness (X_{inh} at the peak magnitude of the second derivative in the curves in Fig. 1) is an order of magnitude higher for TMT (4000 μL/L) than for the iron or manganese (400 μL/L) (as occurs in premixed flames) [6], which is consistent with the higher vapor pressure for the tin compounds. Also, the manner in which Fe-, Sn-, and Mn-containing compounds lose their effectiveness in premixed flames [6] is comparable to that indicated in Fig. 1. Finally, a visible outer annulus, apparently particles, was observed in all flames with added metals, and the blackbody radiation from that region increased with higher agent volume fraction. Separate laser-scattering measurements verified the presence of particles near the reaction zone, and these particles increased in size/number density as the volume fraction of Fe(CO)$_5$ increased.
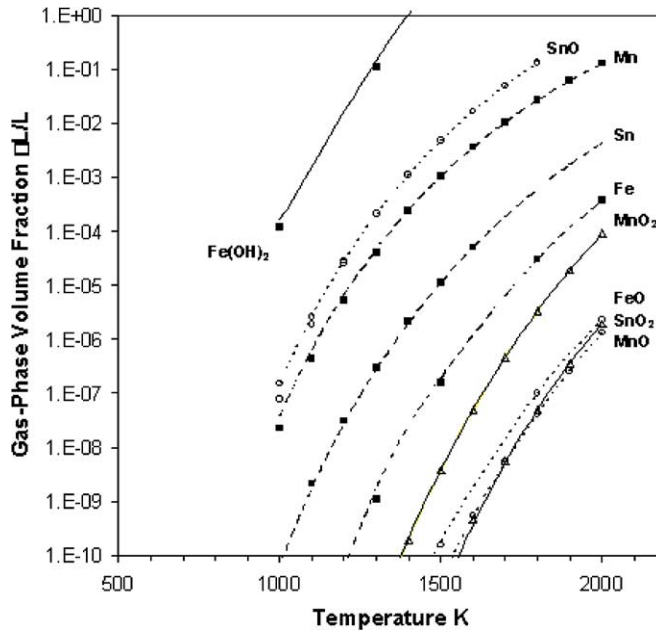
Fig. 11. Metallic species gas-phase volume fraction at equilibrium over the condensed phase (at 1 atm), i.e., vapor pressure, for Fe, Mn, Sn, FeO, MnO, SnO, $Fe(OH)_2$, MnO_2, and SnO_2, from [61].

7.3. Particle formation

The potential for particle formation is investigated by examining the vapor pressure of the condensed-phase metal species that can form in the flame. Fig. 11 shows the equilibrium volume fraction of the gas-phase species over the condensed phase species (at atmospheric pressure) for Fe, Mn, Sn, FeO, MnO, SnO, $Fe(OH)_2$, MnO_2, and SnO_2 from Ref. [61]. (Note: although of interest, condensed-phase thermodynamic data for FeOH, FeO_2, and $Mn(OH)_2$ are not available.) Clearly, for this temperature range (300 to 2000 K) and these species (added at a volume fraction of up to 10^{-3}), the potential for condensation exists, and the characteristics of the specific metal intermediate species are expected to have a large effect on the condensation behavior. A prominent feature in the figure is the large variation in the vapor pressure (3 to 5 orders of magnitude) for the temperature region of 1500 to 2000 K, which is the temperature range of interest for radical-branching reactions in hydrocarbon flames. That is, reasonable variations in the temperature of the stabilization region between flame types will have big effects on the condensation behavior.

To assess which species are more likely to condense, it is necessary to examine not only the vapor pressure, but also the local volume fraction of the species in the flame. For the flames inhibited by $Fe(CO)_5$, the local volume fractions can be estimated from the numerically calculated flame struc-

ture. Fig. 12 (top) shows the volume fraction of the important iron-containing intermediates as a function of radial distance from the burner centerline, for a height above the burner of 4.8 mm (which corresponds to the location of the stabilization region, or reaction kernel), for a methane–air cup-burner flame with 10% CO_2 and 100 μL/L of $Fe(CO)_5$ in the oxidizer stream. The major iron compounds in the region of peak temperature (which also corresponds with the location of peak chain-carrying radical volume fraction) are $Fe(OH)_2$, FeO_2, FeOOH, and FeOH. Interestingly, the volume fractions of the first three of these dip in the region of high radical volume fraction, likely due to the reaction of these species with the radicals (as described previously in Ref. [9] for FeO_2 and $Fe(OH)_2$).

The bottom part of Fig. 12 shows the supersaturation ratio S_i (the ratio of actual volume fraction of species i to the saturation volume fraction at the local temperature) for Fe, FeO, and $Fe(OH)_2$. As described by Frurip and Bauer [62], who studied Fe particle formation, values of S above a critical value $S_{i,c}$ are likely to lead to condensation. For the temperatures of 1600 and 2200 K, they found $S_{i,c}$ to be 10 and 1000, indicating that a high supersaturation was required for particle formation. As Fig. 12 shows, S_{FeO} is about 10^3 near the point of peak temperature, but rises to over 10^5 just outside that region, clearly indicating a condensation potential, which is higher outside the region of peak temperature than within. Similarly, S_{Fe} is also higher outside the high-temperature
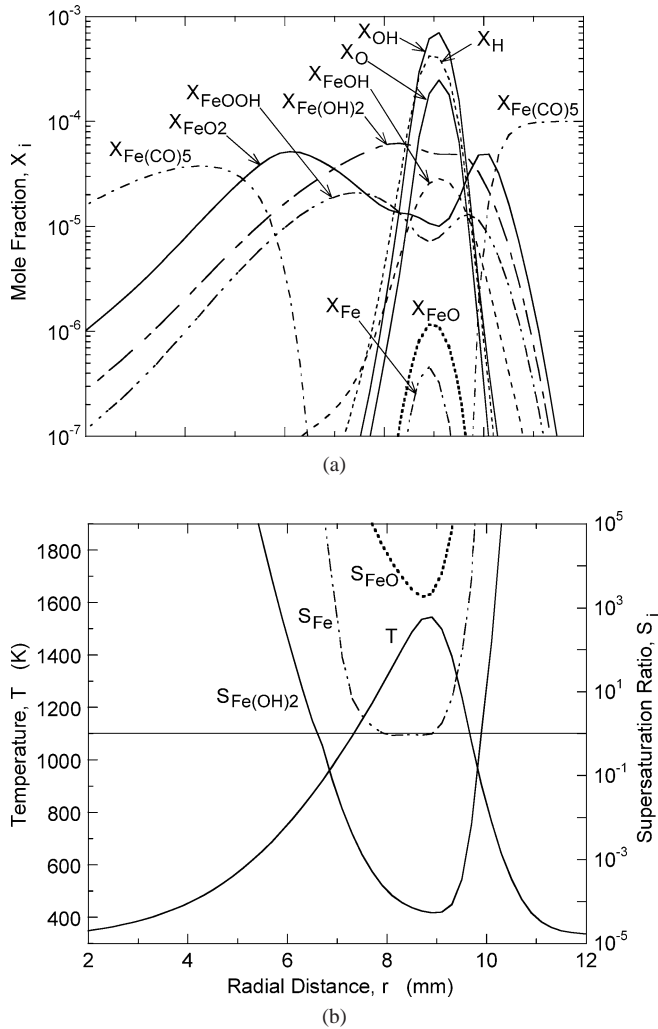
Fig. 12. (a) Calculated iron-containing and major species volume fraction X_i as a function of radial position at a height above the burner of 4.8 mm (corresponding to the location of the reaction kernel in the flame base); and (b) the supersaturation ratio, S_i, for Fe, FeO, and Fe(OH)$_2$.

region than within (10^3 vs 10^0). Nonetheless, the volume fractions of both of these species in the reaction kernel are low ($\leqslant 1$ μL/L), so the potential for significant particle formation is also low, but the analysis reveals the potential for condensation and subsequent re-evaporation in the higher temperature region. Most significant is the curve for Fe(OH)$_2$, which has values of S between 10^{-4} and 10^2 in the temperature range 800 to 1700 K. Since this species accounts for more than half of the iron in the flame, it is likely to condense. Similar analyses were performed at a location further downstream (10 mm) in the flame, a region relatively removed from the stabilization region. There, the effect of the higher peak temperature (~ 1800 K) on the vapor pressure leads to wider physical regions where condensation could occur, and a

higher likelihood (i.e., lower S_i) for re-evaporation at the radial location near the peak temperature (although it is not possible to discern this effect from the contours in Figs. 2–5).

While it is desirable to conduct a similar analysis for other gas-phase iron-containing species that might condense, we were unable to find vapor pressure data for FeOH, FeOOH, and FeO$_2$ (all of which are major iron-containing species within the high-temperature reaction zone). Nonetheless, the present analysis reveals that condensation of iron-containing species and their re-evaporation may account for the lack of particles in the high-temperature region of the flame, as indicated in the experimental data of Figs. 2–5. While particles that re-evaporate can deliver the active iron-containing species back into the gas phase where they

can recombine radicals, it has been found that particle formation only slightly overlapping with the region of radical chain branching can affect the inhibitor's efficiency [11]. Further, particle formation can also lead to convective entrainment of the particles, which effectively sequesters them from reaching the reaction zone of the flame [27].

To interpret the scattering results shown in Figs. 2–5, it is useful to discuss previous results of particle measurements in both Bunsen-type premixed [10] and counterflow diffusion flames [27] seeded with $Fe(CO)_5$. A major finding of those studies was that the formation of particles leads to a loss of iron from active gas-phase inhibiting species to the condensed-phase particles, which are much weaker flame inhibitors. If the characteristics of the flow field (including thermophoresis) allowed the particles to remove iron from the system, the active iron-containing inhibiting species could not reach the regions of high radical volume fraction, and $Fe(CO)_5$ proved to be a poor inhibitor. The main factors found to affect the particle formation were the local temperature, the $Fe(CO)_5$ loading, and the residence time for condensation. At low enough volume fraction, the iron compounds were below their dew point at flame temperatures, so they remained effective in the gas phase. At higher volume fractions, particles were formed. Longer residence times were associated with larger particles and greater loss of effectiveness. This was true for both the premixed flames [10] and the counterflow diffusion flames [27]. The premixed flames had the shortest particle-formation residence times (on the order of 5 ms), and the peak scattering cross section for all of the flames tested with 200 μL/L of added $Fe(CO)_5$ was $1.6 \times 10^{-7} 1/(\text{cm-sr})$ (which is 77 times that of room-temperature air). Some of the counterflow diffusion flame configurations had much larger residence times (on the order of 50 ms), and also had much larger scattering cross sections, up to $4.7 \times 10^{-6} 1/(\text{cm-sr})$, which is about the same as the peak value in the present work (for 200 μL/L of $Fe(CO)_5$). For those counterflow diffusion flames, virtually no flame inhibition was observed.

A key difference between the premixed and counterflow diffusion flames and the present cup-burner flames is the lower temperature of the flame stabilization region of the cup-burner flame. For example, the premixed and counterflow diffusion flames of the previous studies had peak temperatures of 2230 and 1800 to 2000 K, respectively, whereas in the cup-burner flames, the temperature in the reaction kernel is about 1550 K. As shown in Fig. 11, the vapor pressure of the important metal-containing intermediates is very sensitive to the temperature in the range 1000 to 2000 K, indicating that the intermediates will be more likely

to condense and less likely to revaporize in the cup-burner flame. The different flame configurations also have widely differing flow fields, which will lead to different residence times for condensation (which has been shown previously to be an important parameter for particle formation). For example, the cup-burner flames likely have much lower strain rates than the counterflow diffusion flames, leading to much longer flow-field residence times in the cup-burner flames, enhancing the potential for condensation.

7.4. Thermophoresis

A possible cause of the relative loss of effectiveness of $Fe(CO)_5$ in cup-burner flames is the formation of particles followed by flow-field effects which keep the active species from reaching regions relevant to flame inhibition [63]. To examine the role of thermophoresis in the present flames, numerical calculations were performed for a methane–air cup-burner flame with a CO_2 volume fraction of 10% in the oxidizer stream. Particles in the free-molecular regime ($Kn \gg 1$, in which Kn = Knudsen number ≡ [the mean-free path]/[the particle radius]) were introduced into the oxidizer stream at the 800 K isotherm, and their trajectory in the flame was tracked. The thermophoretic velocity is given by the Waldmann equation [64]. Fig. 13 shows the particle tracks for these particles influenced by drag, gravity, and thermophoretic forces. As the figure shows, near the flame base, there is some deviation of the particles both up and down around the reaction kernel; however, examination of the estimated radial and axial thermophoretic velocities shows them to be much less than the gas velocity. Consequently, as indicated in Fig. 13, the particles still pass directly into the reaction kernel, so the effect of thermophoresis near this region is expected to be minor.

8. Conclusions

The first data on the blowoff characteristics of highly effective catalytic agents added with CO_2 to a cup-burner flame of methane and air have been measured. Although such catalytic agents have previously been found to be very effective in premixed and counterflow diffusion flames, they are surprisingly less effective in cup-burner flames. The experiments have shown that for reducing the amount of CO_2 required for blowoff, the order of increasing performance is CF_3Br, TMT, $Fe(CO)_5$, and MMT. Hence, the relative performances of $Fe(CO)_5$ and MMT are switched relative to those in premixed flames. Further, a combination of three organometallic catalytic agents, each at a volume fraction that should reduce the overall
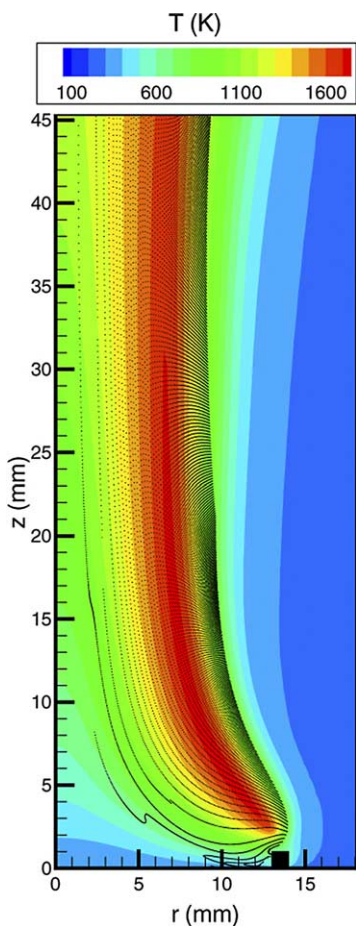
Fig. 13. Calculated particle trajectories for free-molecular-regime particles in a CH_4–air flame with 10% CO_2 in the oxidizer stream.

cles with a peak scattering cross section 1660 times higher than that from air. The particles occur inside and outside of (but not coincident with) the visible flame location, and the scattering signal goes up as the $Fe(CO)_5$ loading increases. The vapor pressure of some important metal-containing intermediate species of Mn, Sn, and Fe was examined. The data reveal that the equilibrium gas-phase volume fraction of these species varies by orders of magnitude in the temperature range of 1000 to 2000 K, also indicating the potential role of condensation and the sensitivity to temperature of the relevant region of the flame.

The first numerical calculations of the flame structure and blowoff conditions for the catalytic flame inhibitor $Fe(CO)_5$ in cup-burner flames were performed. The calculated blowoff condition for methane–air flames with 10% CO_2 and added $Fe(CO)_5$, using a gas-phase-only model, predicted much stronger inhibition of the flames than observed in the experiments (a result consistent with that found previously in counterflow diffusion flames). The calculated flame structure, together with vapor pressure data for key intermediate species, was used to illustrate the potential for particle formation, especially outside of the peak temperature regions. The numerical model was also used to predict the trajectories of particles in the flame. The calculations, which include the effects of thermophoresis (for particles in the free-molecular regime, $Kn \gg 1$), indicate that the particles enter the reaction kernel in the flame base and that thermophoresis does not significantly modify their trajectories.

The relative performance of these very powerful flame inhibitors has been found to be highly dependent upon the type of flame configurations used for the tests, and evidence is presented that the reasons are the varying condensation behavior and blowoff-limit phenomena in the different flame types. Nonetheless, in the absence of condensation, many of the common measures of flame inhibition provide similar ranking of agents with respect to an agent's performance benefit over CO_2.

reaction rate by a factor of 4, reduced the amount of CO_2 required for blowoff by only 25%, a result that was strikingly unexpected. The superior performance of MMT as compared to $Fe(CO)_5$ in the cup burner was explained based on thermodynamic considerations: the volume fractions of the required intermediate species in the catalytic cycle are favored at the lower temperature in the manganese system. At higher volume fractions, each of the metal-based agents experienced a loss of effectiveness that is reminiscent of their behavior in premixed flames. In contrast, the agent Br_2 was effective alone or in combination with CO_2, with a performance improvement over CF_3Br of about a factor of 2.

The loss of effectiveness of the organometallic agents is believed to be caused by particle formation. Laser light-scattering measurements with up to 450 μL/L of $Fe(CO)_5$ in the air stream and CO_2 added at a volume fraction of 8% indicate parti-

References

[1] E.M. Bulewicz, P.J. Padley, Proc. Combust. Inst. 13 (1971) 73.

[2] G. Lask, H.G. Wagner, Proc. Combust. Inst. 8 (1962) 432.

[3] U. Bonne, W. Jost, H.G. Wagner, Fire Res. Abstracts Rev. 4 (1962) 6.

[4] D. Reinelt, G.T. Linteris, Proc. Combust. Inst. 26 (1996) 1421.

[5] G.T. Linteris, M.D. Rumminger, V. Babushok, W. Tsang, Proc. Combust. Inst. 28 (2000) 2965.

[6] G.T. Linteris, K. Knyazev, V. Babushok, Combust. Flame 129 (2002) 221.

[7] NFPA, Clean Agents Fire Extinguishing Systems, 2001, p. 1999.

[8] M.D. Rumminger, D. Reinelt, V. Babushok, G.T. Linteris, Combust. Flame 116 (1999) 207.

[9] M.D. Rumminger, G.T. Linteris, Fire Safety Science: Proc. of the Sixth Int. Symp., Int. Assoc. for Fire Safety Science, Marne-La-Vallee, France, 2000, pp. 289–300.

[10] M.D. Rumminger, G.T. Linteris, Combust. Flame 120 (2000) 451.

[11] M.D. Rumminger, G.T. Linteris, Combust. Flame 123 (2000) 82.

[12] W.A. Rosser, S.H. Inami, H. Wise, Study of the mechanisms of fire extinguishment of liquid rocket propellants, WADC Technical Report 59-206, 1959.

[13] W.A. Rosser, S.H. Inami, H. Wise, Combust. Flame 7 (1963) 107.

[14] E.S. Lippincott, M.C.J. Tobin, J. Am. Chem. Soc. 75 (1953) 4141.

[15] J.L. Lott, S.D. Christian, C.M. Sliepcevich, E.E. Tucker, Fire Technol. 32 (1996) 260.

[16] T. Noto, V. Babushok, A. Hamins, W. Tsang, Combust. Flame 112 (1998) 147.

[17] Y. Saso, Y. Ogawa, N. Saito, H. Wang, Combust. Flame 118 (1999) 489.

[18] M.A. Macdonald, F.C. Gouldin, E.M. Fisher, Combust. Flame 124 (2001) 668.

[19] B.A. Williams, J.W. Fleming, in: Halon Options Technical Working Conference, Center for Global and Environmental Technologies, Albuquerque, NM, 2001, pp. 144–154.

[20] C.P. Fenimore, G.W. Jones, Combust. Flame 10 (1966) 295.

[21] G.T. Linteris, H.K. Chelliah, Powder-matrix systems for safer handling and storage of suppression agents, in: NISTIR, vol. 6766, National Institute of Standards and Technology, Gaithersburg, MD, 2001.

[22] V.R. Katta, L.P. Goss, W.M. Roquemore, AIAA J. 34 (1994) 84.

[23] B. Hirst, K. Booth, Fire Technol. 13 (1977) 296.

[24] G.T. Linteris, G.W. Gmurczyk, in: R.G. Gann (Ed.), Fire Suppression System Performance of Alternative Agents in Aircraft Engine and Dry Bay Laboratory Simulations, National Institute of Standards and Technology, Gaithersburg, MD, 1995, pp. 201–318.

[25] A.G. Gilbert, K.G.P. Sulzmann, J. Electrochem. Soc. 121 (1974) 832.

[26] D.R. Stull, Ind. Eng. Chem. 39 (1947) 517.

[27] M.D. Rumminger, G.T. Linteris, Combust. Flame 128 (2002) 145.

[28] R.R. Rudder, D.R. Bach, J. Opt. Soc. Am. 58 (1968) 1260.

[29] J. Warnatz, in: W.C. Gardiner (Ed.), Combustion Chemistry, Springer-Verlag, New York, 1984, pp. 197–360.

[30] V.R. Katta, W.M. Roquemore, in: Central States Section Meeting/The Combustion Institute, 1996, pp. 449–454.

[31] F. Takahashi, V.R. Katta, Proc. Combust. Inst. 28 (2000) 2071.

[32] J.O. Hirschfelder, C.F. Curtis, R.B. Bird, The Molecular Theory of Gases and Liquids, Wiley, New York, 1954.

[33] F.A. Williams, Combustion Theory, Benjamin/Cummings, Menlo Park, CA, 1985.

[34] Anon, Computational submodels, International Workshop on Measurement and Computation of Turbulent Nonpremixed Flames, http://www.ca.sandia.gov/tdf/ Workshop/Submodels.html, 2001.

[35] V.R. Katta, F. Takahashi, G.T. Linteris, in: Fire Safety Science: Proc. of the Seventh Int. Symp., Int. Assoc. for Fire Safety Science, 2002, pp. 111–999.

[36] H.K. Chelliah, F.A. Williams, Combust. Flame 80 (1990) 17.

[37] F. Takahashi, W.J. Schmoll, Proc. Combust. Inst. 23 (1991) 677.

[38] F. Takahashi, G.T. Linteris, V.R. Katta, in: Fourth International Symposium on Scale Modeling, National Center for Microgravity Research, 2003, pp. 45–54.

[39] R.F. Simmons, H.G. Wolfhard, Combust. Flame 1 (1957) 155.

[40] R. Friedman, Fire Res. Abstracts Rev. 3 (1961) 128.

[41] C.P. Fenimore, Chemistry in Premixed Flames, Pergamon, Oxford, 1964.

[42] R. Friedman, Fire Res. Abstracts Rev. 13 (1971) 187.

[43] J.W. Hastie, J. Res. Natl. Bur. Stand. A. Phys. Chem. A 77 (1973) 733.

[44] F.A. Williams, J. Fire Flammability 5 (1974) 54.

[45] J.W. Hastie, High Temperature Vapors, Academic Press, New York, 1975.

[46] N. Peters, Combust. Sci. Technol. 30 (1983) 1.

[47] H.K. Chelliah, G. Yu, T.O. Hahn, C.K. Law, Proc. Combust. Inst. 24 (1992) 1083.

[48] V. Babushok, W. Tsang, Combust. Flame 123 (2000) 488.

[49] F.G. Roper, Combust. Flame 29 (1977) 219.

[50] K. Seshadri, F.A. Williams, Int. J. Heat Mass Transfer 21 (1978) 137.

[51] T.A. Milne, C.L. Green, D.K. Benson, Combust. Flame 15 (1970) 255.

[52] G.T. Linteris, L. Truett, Combust. Flame 105 (1996) 15.

[53] D. Trees, A. Grudno, N. Ilincic, T. Weissweiler, K. Seshadri, The Joint Spring Meeting, Central/Western/ Mexican Sections of the Combustion Institute, pp. 227–232.

[54] G.T. Linteris, M.D. Rumminger, V. Babushok, H. Chelliah, A.K. Lazzarini, P. Wanigarathne, Effective non-toxic metallic fire suppressants, in: NISTIR,

vol. 6875, National Institute of Standards and Technology, Gaithersburg, MD, 2002.

[55] M. Bundy, A. Hamins, K.Y. Lee, Combust. Flame 133 (2003) 299.

[56] A. Hamins, D. Trees, K. Seshadri, H.K. Chelliah, Combust. Flame 99 (1994) 221.

[57] G.T. Linteris, M.D. Rumminger, Western States Section Meeting, The Combustion Institute, La Jolla, CA, 2002, Paper 030.

[58] F. Takahashi, V.R. Katta, Combust. Sci. Technol. 155 (2000) 243.

[59] M.J. Day, D.V. Stamp, K. Thompson, G. Dixon-Lewis, Proc. Combust. Inst. 13 (1971) 705.

[60] M.D. Rumminger, V.I. Babushok, G.T. Linteris, Proc. Combust. Inst. 29 (2002) 329–336.

[61] L.V. Gurvich, V.S. Iorish, D.V. Chekhovskoi, A.D. Ivanisov, A.Yu. Proskurnev, V.S. Yungman, V.A. Medvedev, I.V. Veits, G.A. Bergman, IVTHANTHERMO—Database on Thermodynamic Properties of Individual Substances, Institute of High Temperatures, Moscow, 1993.

[62] D.J. Frurip, S.H. Bauer, J. Phys. Chem. 81 (1977) 1001.

[63] G.T. Linteris, NRIFD, Tokyo, Japan, 2002.

[64] L. Waldmann, K.H. Schmidt, in: C.N. Davies (Ed.), Aerosol Science, Academic Press, New York, 1966, pp. 137–162.